PHYSICAL REVIEW B **90**, 161110(R) (2014)

# Lattice-tuned magnetism of $Ru^{4+}(4d^4)$ ions in single crystals of the layered honeycomb ruthenates $Li_2RuO_3$ and $Na_2RuO_3$

J. C. Wang,[1,2,3] J. Terzic,[1] T. F. Qi,[1] Feng Ye,[1,2] S. J. Yuan,[1,4] S. Aswartham,[1] S. V. Streltsov,[5,6] D. I. Khomskii,[7] R. K. Kaul,[1] and G. Cao[1,*]

[1]*Center for Advanced Materials, Department of Physics and Astronomy, University of Kentucky, Lexington, Kentucky 40506, USA*
[2]*Quantum Condensed Matter Division, Oak Ridge National Laboratory, Oak Ridge, Tennessee 37831, USA*
[3]*Department of Physics, Renmin University of China, Beijing 100872, China*
[4]*Department of Physics, Shanghai University, Shanghai, China*
[5]*Institute of Metal Physics, 620041 Ekaterinburg, Russia*
[6]*Ural Federal University, 620002 Ekaterinburg, Russia*
[7]*II.Physikalisches Institut, Universitaet zu Koeln, Germany*

(Received 22 August 2014; revised manuscript received 26 September 2014; published 29 October 2014)

We synthesize and study single crystals of the layered honeycomb lattice Mott insulators $Na_2RuO_3$ and $Li_2RuO_3$ with magnetic $Ru^{4+}(4d^4)$ ions. The newly found $Na_2RuO_3$ features a nearly ideal honeycomb lattice and orders antiferromagnetically at 30 K. Single crystals of $Li_2RuO_3$ adopt a honeycomb lattice with either $C2/m$ or more distorted $P2_1/m$ below 300 K, depending on detailed synthesis conditions. We find that $Li_2RuO_3$ in both structures hosts a well-defined magnetic state, in contrast to the singlet ground state found in polycrystalline $Li_2RuO_3$. A phase diagram generated based on our results uncovers a new, direct correlation between the magnetic ground state and basal-plane distortions in the honeycomb ruthenates.

DOI: 10.1103/PhysRevB.90.161110 PACS number(s): 61.05.C−, 71.70.Ej, 75.30.Kz

*Introduction*. It has been of great interest to study interacting electrons on the honeycomb lattice in various contexts both experimentally (e.g., graphene) and theoretically (e.g., the Kitaev model). Studies of honeycomb materials have intensified in recent years [1–19] in part because strong spin-orbit coupling (SOC) along with other competing interactions and geometric frustration in the honeycomb iridates $Na_2IrO_3$ and $Li_2IrO_3$ favors a highly anisotropic Kitaev interaction [20] that stabilizes exotic ground states such as topological spin liquids [1]. It is now experimentally established that $Na_2IrO_3$ exhibits a peculiar zigzag magnetic order at $T_N = 18$ K [5,14,15], and $Li_2IrO_3$ also orders at $T_N = 15$ K but with a different ground state yet to be defined [3,17,21,22,23]. Indeed, for $(Na_{1-x}Li_x)_2IrO_3$ with $0 \leqslant x \leqslant 0.90$, the measured phase diagram demonstrates a dramatic suppression of $T_N$ at intermediate $x$ suggesting that the magnetic order in $Na_2IrO_3$ and $Li_2IrO_3$ is different; however, no spin liquid has been observed thus far [17]. Our pursuit of an understanding of the honeycomb iridates has led us to their ruthenate counterparts, $Na_2RuO_3$ and $Li_2RuO_3$. These materials feature $Ru^{4+}(4d^4)$ ions and a weaker or "intermediate strength" SOC (∼0.16 eV, compared to ∼0.4 eV for Ir ions) [24]. The different $d$-shell filling and contrasting hierarchy of energy scales between the ruthenates and iridates provide a unique opportunity for a deeper understanding of the fundamental problem of interacting electrons on the honeycomb lattices. The magnetism of $Ru^{4+}$ ions as well as other heavy "$d^4$ ions" [such as $Rh^{5+}(4d^4)$, $Re^{3+}(5d^4)$, $Os^{4+}(5d^4)$, and $Ir^{5+}(5d^4)$] is interesting in their own right, as emphasized recently [25]. Materials with heavy $d^4$ ions tend to adopt a low-spin state because larger cubic-crystal fields often overpower the Hund's rule coupling. On the other hand, SOC with the intermediate strength may still be strong enough to impose a competing, singlet ground state or an angular momentum $J = 0$ state. Novel magnetic states may thus emerge when the singlet-triplet splitting (0.05–0.20 eV) becomes comparable to exchange interactions (0.05–0.10 eV) and/or noncubic crystal fields [25–27]. This is evidenced in a recent study of materials containing $5d^4$ ions [28].

Up until now, no physical and structural properties of $Na_2RuO_3$ have been investigated but a few experimental and theoretical studies of polycrystalline $Li_2RuO_3$ have been reported in recent years [29–32]. In essence, polycrystalline $Li_2RuO_3$ undergoes a structural phase transition near $T_D = 540$ K that features a change of space group from $C2/m$ (No. 12) at high temperatures to $P2_1/m$ (No. 11) at low temperatures. The low-temperature phase adopts a strongly distorted honeycomb lattice, which prompts a simultaneous dimerization that results in a singlet ground state [29]. The observation of dimerized zigzag chains has recently stimulated more investigations of $Li_2RuO_3$ [30–32], in which the dimerization is attributed to orbital ordering [29], creation of valence bond crystal [30], and Jahn-Teller distortions [31], respectively. It is noted that all reported experimental results were culled from polycrystalline $Li_2RuO_3$ [29,31,32].

Here we report structural, magnetic, and thermal properties of single-crystal $Li_2RuO_3$ and $Na_2RuO_3$. The newly found $Na_2RuO_3$ with space group $C2/m$ features a nearly ideal honeycomb lattice and orders antiferromagnetically below 30 K. It may serve as a reference for almost perfect honeycomb symmetry. On the other hand, single-crystal $Li_2RuO_3$ adopts a less ideal honeycomb lattice with either $C2/m$ or more distorted $P2_1/m$ below 300 K but both phases exhibit a well-defined, though different, magnetic state, which sharply contrasts with the singlet ground state due to dimerization observed in polycrystalline $Li_2RuO_3$ [29]. This work produces a phase diagram that uncovers a direct correlation between the ground state and basal-plane distortions or lattice-tuned

*Corresponding author: cao@uky.edu

 

TABLE I. Structural comparison between the honeycomb lattices at 100 K.

| Compound | Space group | $a$ (Å) | $b$ (Å) | $b/a$ | $(L_l-L_s)/L_s$ |
|---|---|---|---|---|---|
| $Li_2RuO_3$ (Powder)[a] | $P2_1/m$ | 4.9210(2) | 8.7829(2) | 1.785 | 18.6% |
| $Li_2RuO_3$ ($P$) | $P2_1/m$ | 4.963(3) | 8.766(6) | 1.766 | 10.1% |
| $Li_2RuO_3$ ($C$) | $C2/m$ | 5.021(4) | 8.755(6) | 1.744 | 2.1% |
| $Na_2RuO_3$ | $C2/m$ | 5.346(1) | 9.255(2) | 1.731 | 0.17% |
| $(Li_{0.9}Na_{0.1})_2IrO_3$ | $C2/m$ | 5.186(1) | 8.964(2) | 1.728 | 0.6% |
| $Na_2IrO_3$ | $C2/m$ | 5.319(1) | 9.215(2) | 1.732 | 0.14% |

[a]Taken at 300 K.

magnetism in all honeycomb ruthenates studied. (Both $Li_2RuO_3$ and $Na_2RuO_3$ are highly insulating; their transport properties are not included in this Rapid Communication.)

*Crystal structures*. Single crystals of $Li_2RuO_3$ and $Na_2RuO_3$ were synthesized using the self-flux method, which is described elsewhere [17]. For synthesis of single-crystal $Li_2RuO_3$ the mixed chemicals were first heated up to 1250 °C and then cooled to 900 °C at 2 °C/h and finally room temperature at 50 °C/h. In contrast, the polycrystalline $Li_2RuO_3$ was synthesized at a much lower temperature of 950 °C. The different synthesis conditions may have important implications for the ground state of $Li_2RuO_3$. For more experimental details, see the Supplemental Material [33]. Crystal structures on which the ground state so sensitively hinges require a close examination. Table I includes the lattice parameters of single-crystal $Li_2RuO_3$ and $Na_2RuO_3$ as well as those of polycrystalline $Li_2RuO_3$ and iridate counterparts for contrast and comparison. For the sake of discussion, single-crystal $Li_2RuO_3$ with $C2/m$ and $P2_1/m$ are labeled as $Li_2RuO_3$ ($C$) and $Li_2RuO_3$ ($P$), respectively. A major distinction between $Li_2RuO_3$ ($C$) and $Li_2RuO_3$ ($P$) is the number of unequal Ru-Ru bond distances, which measures distortions that in turn dictate the ground state. $Li_2RuO_3$ ($C$) features two bond distances, or a long and short one, $L_l$ and $L_s$, respectively, whereas $Li_2RuO_3$ ($P$) has three bond distances, i.e., $L_l$, $L_s$, and a medium bond distance, $L_m$. The basal-plane distortion is characterized by the

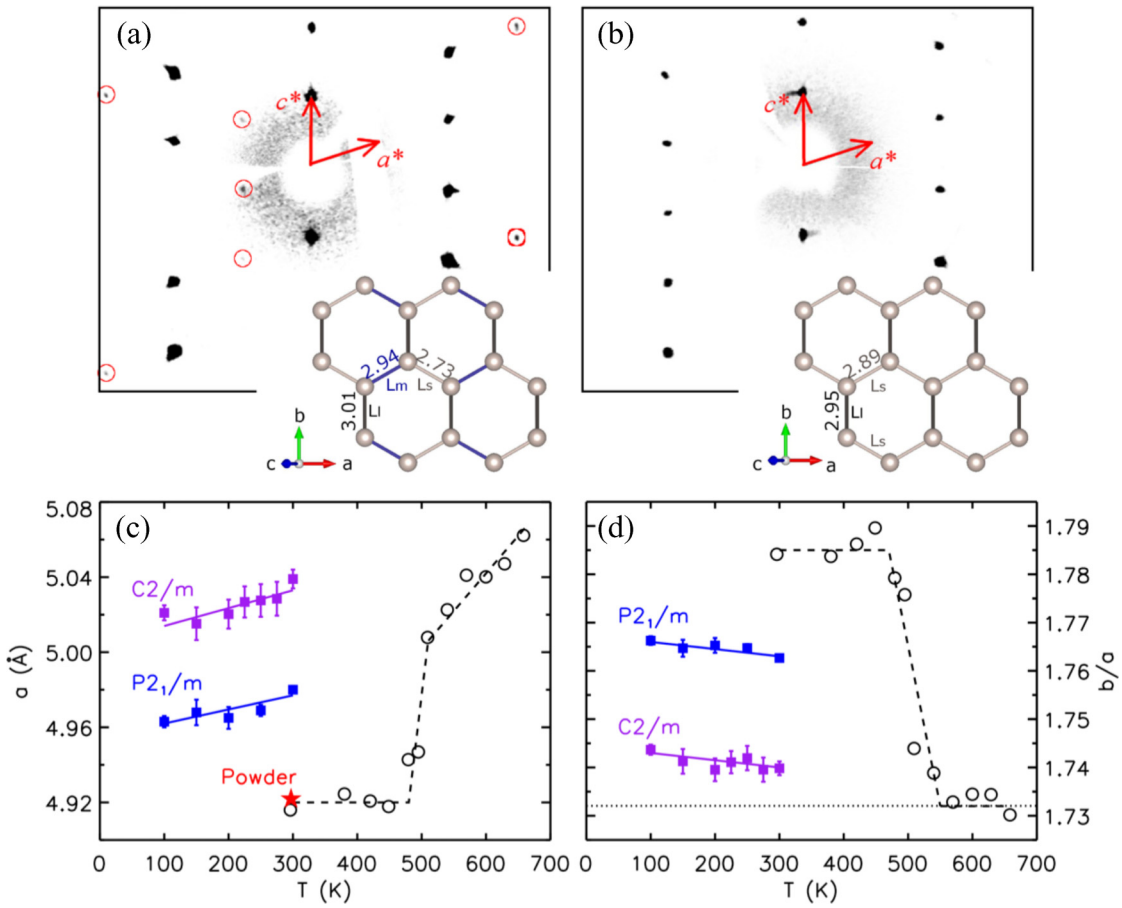


FIG. 1. (Color online) Diffraction images in the ($h0l$) plane of the single-crystal $Li_2RuO_3$ with space group (a) $P2_1/m$ and (b) $C2/m$. Insets: The corresponding honeycomb lattice and Ru-Ru bond distances. The temperature dependence of (c) the $a$ axis and (d) the ratio $b/a$ from our single-crystal $P2_1/m$ phase (blue), $C2/m$ phase (purple), powder samples (red star), and powder data from Ref. [29] (black circles). Note that the sharp diffraction pattern clearly indicates the high quality of the single-crystal $Li_2RuO_3$.

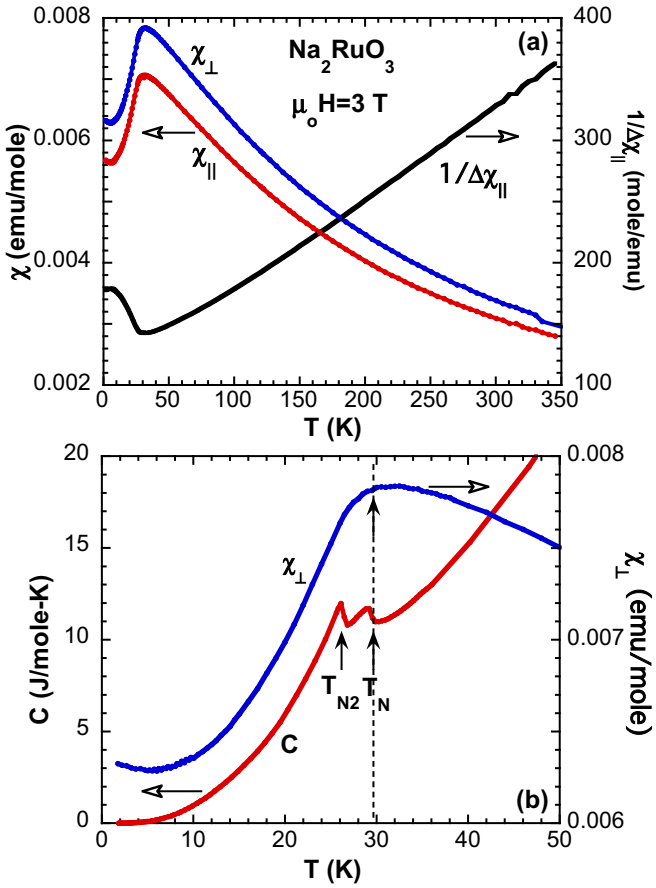


FIG. 2. (Color online) Single-crystal $Na_2RuO_3$: (a) The temperature dependence of the magnetic susceptibility for the basal plane $\chi_{\|}(T)$ and out-of-plane $\chi_{\perp}(T)$ for single-crystal $Na_2RuO_3$; Right scale: $1/\Delta\chi_{\|}$ where $\Delta\chi = \chi - \chi_o$ and $\chi_o$ is the temperature-independent contribution to $\chi$. (b) The temperature dependence of the specific heat $C(T)$ and $\chi_{\perp}(T)$ (right scale).

bond difference ratio defined as $(L_l - L_s)/L_s$, which is shown in Table I, and Figs. 1(a) and 1(b). In general, honeycomb lattices with $C2/m$ tend to have a larger $a$-axis lattice parameter and smaller ratio $b/a$ ($\sim\sqrt{3}$) than those with $P2_1/m$, thus less distorted. Figures 1(c) and 1(d) demonstrate the lattice parameters of single-crystal and polycrystalline samples as a function of temperature. As seen, no structural transition is discerned in the single crystals studied for the temperature range measured. In short, the structural differences between the polycrystalline $Li_2RuO_3$ and $Li_2RuO_3$ ($C$) or $Li_2RuO_3$ ($P$) are distinguished by the different space groups or by the difference in $(L_l - L_s)/L_s$. It is clear that $Li_2RuO_3$ ($P$) is more distorted than $Li_2RuO_3$ ($C$) but much less distorted than the polycrystalline sample despite the same space group shared by both (Table I).

*Physical properties*. $Na_2RuO_3$ exhibits a sharp antiferromagnetic (AFM) transition at $T_N = 30$ K, as shown in Fig. 2(a). The magnetic anisotropy leads to a stronger out-of-plane magnetic susceptibility $\chi_{\perp}$ than in-plane magnetic susceptibility $\chi_{\|}$. The linearity illustrated in $1/\Delta\chi_{\|}$ [right scale in Fig. 2(a)] indicates that the data fit well with the Curie-Weiss law for $100 < T < 350$ K, and yield the Curie-Weiss temperature $\theta_{CW} = -137$ K and effective moment $\mu_{eff} = 2.45\mu_B$/Ru (Table II). The frustration parameter defined as FP $= |\theta_{CW}|/T_N$ is estimated to be 4.6. This value suggests a presence of modest frustration, comparable to that for its iridate counterpart.

TABLE II. Physical parameters of the single-crystal honeycomb lattices. FP stands for frustration parameter.

| Compound | $T_N$ (K) | $\theta_{CW}$ (K) | FP | $\mu_{eff}$ ($\mu_B$/Ru or Ir) |
|---|---|---|---|---|
| $Li_2RuO_3$ ($P$) | ~5 | −58 | 11.6 | 1.46 |
| $Li_2RuO_3$ ($C$) | 9 | −112 | 12.4 | 2.77 |
| $Na_2RuO_3$ | 30 | −137 | 4.6 | 2.45 |
| $(Li_{0.9}Na_{0.1})_2IrO_3$ | 7 | −18 | 2.6 | 1.95 |
| $Na_2IrO_3$ | 18 | −119 | 6.6 | 1.76 |

The magnetic ordering is confirmed by the specific heat $C(T)$ [Fig. 2(b)]. However, an additional peak at $T_{N2} = 26$ K that is absent in $\chi(T)$ is also seen in $C(T)$. This behavior, which is reproducible, is remarkably similar to that observed in $Na_2IrO_3$ where an additional, weaker anomaly in $C(T)$ is discerned at $T^* = 21$ K that is followed by the zigzag order at $T_N = 18$ K [15,17]. This two-step transition is discussed in the context of the Kitaev-Heisenberg model on the hexagonal lattice [34]. A similar argument could be applied to $Na_2RuO_3$ although the origin of this magnetic behavior needs to be further investigated. The $C(T)$ data also indicate that the entropy removal due to the two-step magnetic transition is small, less than 10% of $R$ ln3 expected for an $S = 1$ magnet. This implies that the magnetic ordering may not be fully developed perhaps in part because of the tendency of SOC to impose a singlet state. Application of magnetic field up to 14 T causes no visible changes in both $C(T,H)$ and $\chi(T,H)$.

The magnetic properties of both single-crystal $Li_2RuO_3$ ($C$) and $Li_2RuO_3$ ($P$) are examined for $1.7 < T < 900$ K. Neither shows the singlet ground state observed in the polycrystalline $Li_2RuO_3$. Instead, $Li_2RuO_3$ ($C$) displays paramagnetic behavior at $T > 20$ K with the magnetic susceptibility $\chi$ following the Curie-Weiss law for $20\ \text{K} < T \leqslant 750$ K [Fig. 3(a)]. Data fits to the Curie-Weiss law yield an effective moment $\mu_{eff} = 2.77\mu_B$/Ru, consistent with that expected for an $S = 1$ system, and a Curie-Weiss temperature $\theta_{CW} = -112$ K. A signature for a long-range order near $T_N = 9$ K is evident in both $\chi(T)$ and $C(T)$ [Fig. 3(b)]. A large frustration parameter, FP $= |\theta_{CW}|/T_N = 12.4$ suggests the presence of significant frustration (Table II). Indeed, the two unequal Ru-Ru bonds may favor a formation of zigzag chains along the $a$ axis (see schematic in the inset of Fig. 4) as the interchain interaction is weak due to the long Ru-Ru bond $L_l$. Therefore, no magnetic ordering occurs until below $T_N = 9$ K when three-dimensional correlations are established.

For more distorted $Li_2RuO_3$ ($P$), a magnetically ordered state also takes place but at a lower temperature, $T_N = 4$ K [Figs. 3(c) and 3(d)]. Remarkably, the magnetic anisotropy is much stronger, and the magnitude of $\chi_{\perp}$ is significantly larger than that in $Li_2RuO_3$ ($C$), implying the importance of SOC. However, the temperature dependence of $\chi$ at high temperatures is much weaker than that for $Li_2RuO_3$ ($C$). The results suggest that $Li_2RuO_3$ ($P$) is "halfway" to dimerization

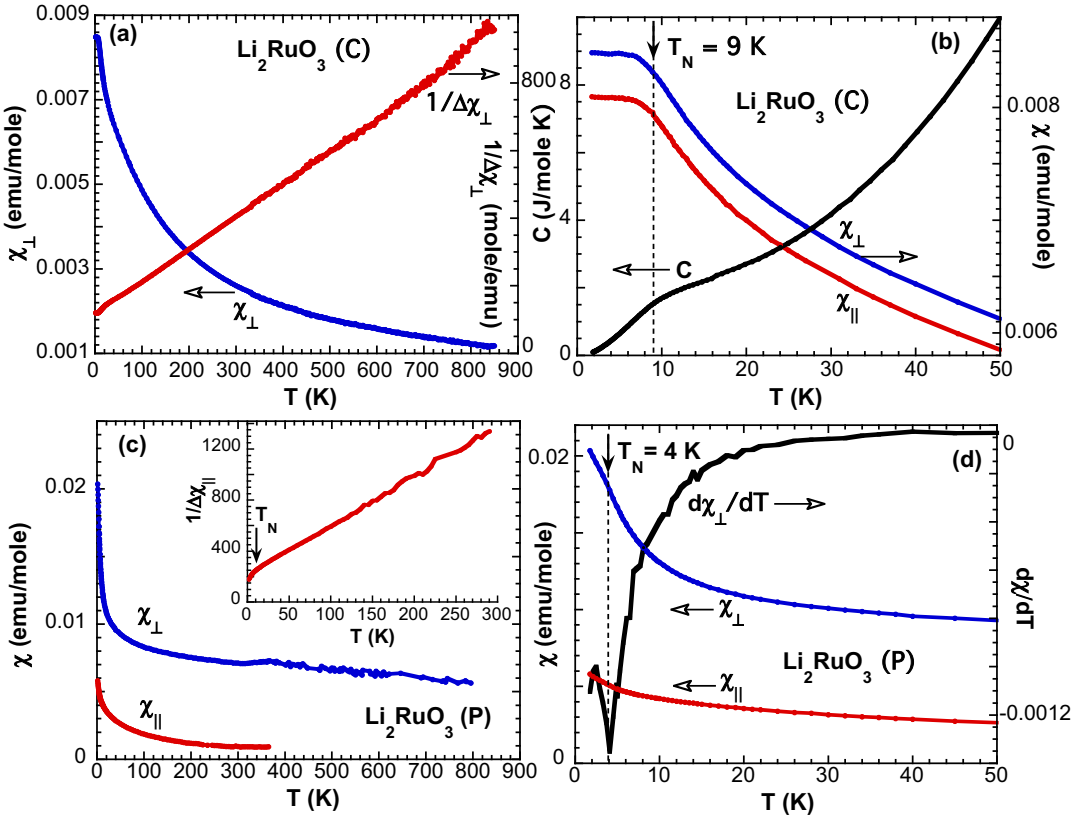


FIG. 3. (Color online) Single-crystal $Li_2RuO_3$ ($C$): The temperature dependence of (a) the magnetic susceptibility $\chi_{\|}(T)$ and $\chi_{\perp}(T)$ and $1/\Delta\chi_{\perp}$ (right scale) for $1.7 < T < 850$ K and (b) the specific heat $C(T)$ and $\chi_{\|}(T)$ and $\chi_{\perp}(T)$ (right scale) at low $T$. Single-crystal $Li_2RuO_3$ ($P$): The temperature dependence of (c) $\chi_{\|}(T)$ and $\chi_{\perp}(T)$ and $1/\Delta\chi_{\perp}$ (inset) and (d) $\chi_{\|}(T)$ and $\chi_{\perp}(T)$ and $d\chi_{\perp}/dT$ (right scale) at low $T$.

as the lattice is more similar to that of the polycrystalline sample; the magnetic state eventually prevails below $T_N = 4$ K because $Li_2RuO_3$ ($P$) is after all not as distorted as the polycrystalline $Li_2RuO_3$.

*Computational results*. Our LDA (local density approximation) calculations using the LMTO (linearized muffin-tin orbitals) method [35] and Wannier function projection method [36] show that the crystal-field splitting in the Ru $t_{2g}$ shell does not exceed 70 meV, indicating that the comparable

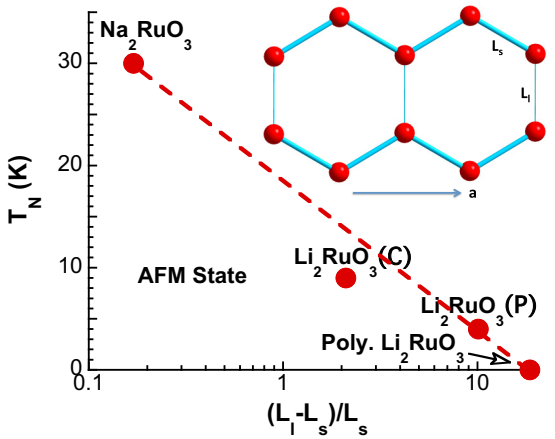


FIG. 4. (Color online) The Néel temperature $T_N$ as a function of the bond distance ratio $(L_l - L_s)/L_s$ for all honeycomb ruthenates. Inset: A schematic of the honeycomb lattice featuring $L_l$ and $L_s$.

SOC may play a significant role. However, the off-diagonal matrix elements of the Hamiltonian, hopping parameters are even larger, ~200 meV, which is strong enough to form the quasimolecular orbitals (QMOs) similar to those in $Na_2IrO_3$ where QMOs involve six Ir atoms arranged in a hexagon and each Ir atom belongs to three different QMOs, which dominate the formation of electronic structure [13] (see Fig. 2. in [33] for band structures of $Na_2RuO_3$ and $Li_2RuO_3$). The results of the optimization of the crystal structure performed in the GGA (generalized gradient approximation) calculations using the pseudopotential method [37] indicate that the nearly ideal honeycomb $Na_2RuO_3$ indeed corresponds to a minimum of the total energy for a zigzag AFM state, in which the magnetic moment on Ru ions is 1.31 $\mu_B$. In addition, our LMTO LDA + $U$ calculations show that a relatively small on-site Coulomb repulsion $U \sim 1.5$ eV is sufficient to suppress the dimerization observed in polycrystalline $Li_2RuO_3$. The band structure of single-crystal $Li_2RuO_3$ strongly differs from that of both $Na_2RuO_3$ and $Na_2IrO_3$ on the LDA level (see Supplemental Material Fig. 2 [33]) and consequently, there is no sign of the QMOs. According to a recent study [31], when one of the QMOs (of $E_{2u}$ symmetry) is half-filled, the corresponding instability may induce the Jahn-Teller distortions (JTDs) that in turn lead to the dimerization. In less distorted single-crystal $Li_2RuO_3$, no sign of the JTDs is seen since the formation of the zigzag chains effectively removes the orbital degeneracy or JTDs. Therefore the zigzag chains constitute an alternative state to the dimerization when

the JTDs are absent. However, both the zigzag chains and dimerized lattice cost certain elastic energy that tends to stabilize uniform structure, and the prevailing state sensitively depends on details of the band structure and bulk modulus of the system (see Supplemental Material [33] for details).

Indeed, all relevant energies vigorously compete and critically bias their mutual competition to stabilize ground states. This explains that there exist nearly degenerate states in these materials, and the prevailing ground state critically depends on details of the structure, as illustrated in Fig. 4. The magnetic ordering systematically decreases with increasing $(L_l - L_s)/L_s$ and eventually vanishes at a critical value where the dimerization emerges, leading to the singlet ground state observed in polycrystalline $Li_2RuO_3$. All results strongly indicate a direct correlation between the ground state and basal-plane distortions. The newly found $Na_2RuO_3$ provides a reference for almost perfect honeycomb symmetry.

The absence of the dimerization in single-crystal $Li_2RuO_3$ cannot be due to either impurity or quality of the single crystals. In fact, the singlet ground state is unusually resilient to heavy impurity doping and is even enhanced by 5% Na doping (see Fig. 3 in the Supplemental Material [33]) and survives up to 50% Ir substitution for Ru in the polycrystalline samples [32]. It is likely that the difference between the two forms of $Li_2RuO_3$ arises from different synthesis conditions, as discussed above, which might cause different degrees of site disorder in the honeycomb network due to the similar ionic radius of Li and Ru, and/or slightly different stoichiometry (e.g., oxygen content) (see Supplemental Material [33]). Hence, this work does not rule out the possibility that single-crystal $Li_2RuO_3$ having the same structural distortions and singlet ground state as polycrystalline $Li_2RuO_3$ may eventually form under certain synthesis conditions.

The work also offers the following general observations. Both $Li_2RuO_3$ and $Li_2IrO_3$ are more structurally distorted and behave with more complexities than their Na counterparts. SOC is expected to impose a $J = 0$ state for $Ru^{4+}(4d^4)$ ions [and a $J_{\text{eff}} = 1/2$ state for $Ir^{4+}(5d^5)$ ions] but the observed magnetic states in the honeycomb ruthenates as in many other ruthenates [24] indicate that SOC is not sufficient to induce a $J = 0$ state. It is intriguing that all honeycomb ruthenates and iridates magnetically order in a similar temperature range (see Supplemental Material Fig. 4 [33]) despite the different role of SOC in them.

*Acknowledgments*. G.C. is thankful to Dr. Natalie Perkins and Dr. Y. B. Kim for discussions. S.S. and D.K. are grateful to Dr. Igor Mazin, Dr. Harald Jeschke, Dr. Roser Valenti, and Dr. Je-Geun Park. This work was supported by the National Science Foundation via Grants No. DMR-0856234, No. DMR-1265162, and No. DMR-1056536 (R.K.K.), Russian Science Foundation via RSCF Grant No. 14-22-00004 (S.V.S.), German project FOR 1346, Cologne University via German excellence initiative (D.K.), DOE BES Office of Scientific User Facilities (F.Y.), and China Scholarship Council (J.C.W.).

[1] G. Jackeli and G. Khaliullin, Phys. Rev. Lett. **102**, 017205 (2009).
[2] Y. Singh and P. Gegenwart, Phys. Rev. B **82**, 064412 (2010).
[3] Y. Singh, S. Manni, J. Reuther, T. Berlijn, R. Thomale, W. Ku, S. Trebst, and P. Gegenwart, Phys. Rev. Lett. **108**, 127203 (2012).
[4] J. Chaloupka, G. Jackeli, and G. Khaliullin, Phys. Rev. Lett. **105**, 027204 (2010).
[5] S. K. Choi, R. Coldea, A. N. Kolmogorov, T. Lancaster, I. I. Mazin, S. J. Blundell, P. G. Radaelli, Y. Singh, P. Gegenwart, K. R. Choi *et al.*, Phys. Rev. Lett. **108**, 127204 (2012).
[6] I. Kimchi and Y.-Z. You, Phys. Rev. B **84**, 180407 (2011).
[7] Y.-Z. You, I Kimchi, and A. Vishwanath, Phys. Rev. B **86**, 085145 (2012).
[8] T. Hyart, A. R. Wright, G. Khaliullin, and B. Rosenow, Phys. Rev. B **85**, 140510 (2012).
[9] C. C. Price and N. B. Perkins, Phys. Rev. Lett. **109**, 187201 (2012).
[10] J. Chaloupka, G. Jackeli, and G. Khaliullin, Phys. Rev. Lett. **110**, 097204 (2013).
[11] H.-S. Kim, C. H. Kim, H. Jeong, H. Jin, and J. Yu, Phys. Rev. B **87**, 165117 (2013).
[12] S. Bhattacharjee, S.-S. Lee, and Y. B. Kim, New J. Phys. **14**, 073015 (2012).
[13] I. I. Mazin, H. O. Jeschke, K. Foyevtsova, R. Valenti, and D. I. Khomskii, Phys. Rev. Lett. **109**, 197201 (2012).
[14] X. Liu, T. Berlijn, W.-G. Yin, W. Ku, A. Tsvelik, Y.-J. Kim, H. Gretarsson, Y. Singh, P. Gegenwart, and J. P. Hill, Phys. Rev. B **83**, 220403 (2011).
[15] F. Ye, S. Chi, H. Cao, B. C. Chakoumakos, J. A. Fernandez-Baca, R. Custelcean, T. F. Qi, O. B. Korneta, and G. Cao, Phys. Rev. B **85**, 180403 (2012).
[16] H. Gretarsson, J. P. Clancy, X. Liu, J. P. Hill, E. Bozin, Y. Singh, S. Manni, P. Gegenwart, J. Kim, A. H. Said *et al.*, Phys. Rev. Lett. **110**, 076402 (2013).
[17] G. Cao, T. F. Qi, L. Li, J. Terzic, V. S. Cao, S. J. Yuan, M. Tovar, G. Murthy, and R. K. Kaul, Phys. Rev B **88**, 220414(R) (2013).
[18] I. Felner and I. Bradaric, Physica B **311**, 195 (2002).
[19] Yuriy Sizyuk, Craig Price, Peter Wolfle, and Natalia B. Perkins, arXiv:1408.3647.
[20] A. Kitaev, Ann. Phys. **321**, 2 (2006).
[21] A recent neutron study by Feng Ye and G. Cao found no sign of a zigzag magnetic structure in $(Na_{0.1}Li_{0.9})_2IrO_3$.
[22] Radu Coldea (private communication).
[23] Johannes Reuther, Ronny Thomale, and Stephan Rachel, Phys. Rev. B **90**, 100405(R) (2014).
[24] Gang Cao and Lance E. DeLong, *Frontiers of 4d- and 5d-Transition Metal Oxides* (World Scientific, Singapore, 2013).
[25] Giniyat Khaliullin, Phys. Rev. Lett. **111**, 197201 (2013).
[26] G. Chen, L. Balents, and A. P. Schnyder, Phys. Rev. Lett. **102**, 096406 (2009).
[27] O. Nganba Meetei, William S. Cole, Mohit Randeria, and Nandini Trivedi, arXiv:1311.2823.
[28] G. Cao, T. F. Qi, L. Li, J. Terzic, S. J. Yuan, L. E. DeLong, G. Murthy, and R. K. Kaul, Phys. Rev. Lett. **112**, 056402 (2014).

[29] Y. Miura, Y. Yasui, M. Sato, N. Igawa, and K. Kakurai, J. Phys. Soc. Jpn. **76**, 033705 (2007).

[30] G. Jackeli and D. I. Khomskii, Phys. Rev. Lett. **100**, 147203 (2008).

[31] Simon A. J. Kimber, I. I. Mazin, Juan Shen, Harald O. Jeschke, Sergey V. Streltsov, Dimitri N. Argyriou, Roser Valenti, and Daniel I. Khomskii, Phys. Rev. B **89**, 081408(R) (2014).

[32] Hechang Lei, Wei-Guo Yin, Zhicheng Zhong, and Hideo Hosono, Phys. Rev. B **89**, 020409(R) (2014).

[33] See Supplemental Material at http://link.aps.org/supplemental/10.1103/PhysRevB.90.161110 for more detailed experimental and computational results.

[34] Crag Price and Natalia B. Perkins, Phys. Rev. B **88**, 024410 (2013).

[35] O. K. Andersen and O. Jepsen, Phys. Rev. Lett. **53**, 2571 (1984).

[36] S. V. Streltsov, A. S. Mylnikova, A. O. Shorikov, Z. V. Pchelkina, D. I. Khomskii, and V. I. Anisimov, Phys. Rev. B **71**, 245114 (2005).

[37] G. Kresse and J. Furthmüller, Phys. Rev. B **54**, 11169 (1996).